Microstructure and microhardness of OFHC copper processed by High-pressure torsion

Abdulla I. Almazrouee, Khaled J. Al-Fadhalah, Saleh N. Alhajeri, Terence G. Langdon

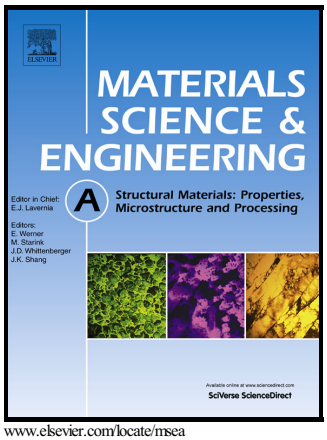

www.elsevier.com/locate/msea

PII: S0921-5093(15)30071-X
DOI: http://dx.doi.org/10.1016/j.msea.2015.06.016
Reference: MSA32454

To appear in: *Materials Science & Engineering A*

Received date: 19 February 2015
Revised date: 16 April 2015
Accepted date: 4 June 2015

Cite this article as: Abdulla I. Almazrouee, Khaled J. Al-Fadhalah, Saleh N. Alhajeri and Terence G. Langdon, Microstructure and microhardness of OFHC copper processed by High-pressure torsion, *Materials Science & Engineering A,* http://dx.doi.org/10.1016/j.msea.2015.06.016

Submitted to Materials Science and Engineering A (February 2015): revised April 2015

Microstructure and microhardness of OFHC copper processed by high-pressure torsion

Abdulla I. Almazrouee[a,*], Khaled J. Al-Fadhalah[b], Saleh N. Alhajeri[a], Terence G. Langdon[c,d,*]

[a]Department of Manufacturing Engineering, College of Technological Studies, P.A.A.E.T., P.O. Box 42325, Shuwaikh 70654, Kuwait

[b]Department of Mechanical Engineering, College of Engineering & Petroleum, Kuwait University, P.O. Box 5969, Safat 13060,Kuwait

[c]Materials Research Group, Faculty of Engineering and the Environment, University of Southampton, Southampton SO17 1BJ, UK

[d]Departments of Aerospace & Mechanical Engineering and Materials Science, University of Southern California, Los Angeles, CA 90089-1453, USA

Abstract

An ultra-high purity oxygen free high conductivity (OFHC) Cu was investigated to determine the evolution of microstructure and microhardness during processing by high-pressure torsion (HPT). Disks were processed at ambient temperature, the microstructures were observed at the center, mid-radius and near-edge positions and the Vickers microhardness was recorded along radial directions. At low strains, Σ3 twin boundaries are formed due to dynamic recrystallization before microstructural refinement and ultimately a stabilized ultrafine grain structure is formed in the near-edge position with an average grain size of ~280 nm after 10 turns. Measurements show the microhardness initially increases to ~150 Hv at an equivalent strain of ~2, then falls to about ~80 Hv during dynamic recrystallization up to a strain of ~8 and thereafter increases again to a saturated value of ~150 Hv at strains above ~22. The delay in microstructure and microhardness homogeneity by dynamic recrystallization is attributed to the high purity of Cu that enhances dislocation mobility and causes dynamic softening during the early stages of straining.

Keywords: HPT, microhardness, microstructure, OFHC copper, recrystallization

*Corresponding authors: T.G. Langdon: e-mail: langdon@usc.edu; A.I. Almazrouee: e-mail: aalmazro1@gmail.com

1. Introduction

The processing of ultrafine-grained (UFG) metals, with grain sizes in the submicrometer or nanometer range, has become of major importance over the last two decades [1-3], primarily because these materials generally exhibit superior properties including high strength and, if there is reasonable microstructural stability at elevated temperatures, they provide an opportunity to achieve a superplastic forming capability. Several different procedures are now available for processing UFG metals through the application of severe plastic deformation (SPD) [4-6] but generally most UFG materials are produced using either equal-channel angular pressing (ECAP) [7] or high-pressure torsion (HPT) [8]. In ECAP the sample is in the form of a rod or bar and it is pressed through a die constrained within a channel having a sharp angle near the center of the die whereas in HPT the sample is usually in the form of a thin disk and it is subjected to a high applied pressure and concurrent torsional straining. Although both procedures have been used to produce UFG microstructures in a wide range of metals, the experimental evidence shows that, by comparison with ECAP, processing by HPT produces both small grains and a higher fraction of grain boundaries having high angles of misorientation [9-11].

In practice, the processing of a disk by HPT introduces a potential difficulty in data analysis because the equivalent von Mises strain, ε_{eq}, is given by the relationship [12]

$$\varepsilon_{eq} = \frac{2\pi Nr}{h\sqrt{3}} \qquad (1)$$

where N is the total number of turns, r is the radial distance from the center of the disk and h is the height (or thickness) of the disk. It follows from eq. (1) that the strain varies across the disk from a maximum value at the edge to a strain of zero at the central point where r = 0.

This suggests that the microstructures achieved after HPT will exhibit considerable inhomogeneities but in practice early experiments on pure Ni, conducted using a combination of microhardness measurements, transmission electron microscopy (TEM) and orientation imaging microscopy (OIM), showed that good homogeneity and an equiaxed microstructure was attained after processing through 5 turns under an applied pressure of 6.0 GPa [13]. It has been demonstrated theoretically, using strain gradient plasticity modeling, that there is a gradual evolution in the hardness values in HPT processing with increasing torsional straining and ultimately these hardness values achieve an essentially uniform distribution [14].

Early measurements in HPT processing showed that the hardness values increase rapidly around the edges of the disks in the early stages of processing and in the central region the evolution in hardness occurs more slowly although ultimately, after a sufficient number of turns, it is generally possible to achieve similar values of hardness throughout the disks [13,15,16]. This trend, in which the hardness increases to a plateau value, is termed hardening without recovery and it represents the general trend for almost all metals: a detailed description of this type of hardening was given in a recent review [17].

By contrast to this general trend, a comprehensive set of experiments conducted on high purity (99.99%) aluminum showed that the hardness was initially higher, rather than lower, in the central region of the disk but these hardness values decreased with further straining and again there was a gradual evolution towards a plateau hardness [18]. These higher initial hardness values in the centers of the disks matched the smaller grains observed in this region by TEM and the development of larger grains at the disk peripheries was attributed to the occurrence of rapid recovery due to the high stacking fault energy (SFE) in pure Al and the consequent rapid recovery through processes such as cross-slip. The development of a high initial hardness at very low strains and the subsequent decrease in

hardness to a lower plateau value is designated softening with rapid recovery [17] and later it was fully documented in experiments on high purity Al where the HPT processing was performed through fractional numbers of revolutions between 1/8 and 1 turn [19,20] or hardness values were recorded on different sectional planes throughout the disks [21]. The occurrence of softening with rapid recovery appears to be almost unique to high purity aluminum because aluminum of lower purity (99.7%) [22] and numerous Al-based alloys [23-33] exhibit conventional hardening without recovery. Nevertheless, there are two recent reports of softening with rapid recovery in the h.c.p. metals of pure (99.9%) Mg [34] and pure (99.99%) Zn [35]. It is important to note that softening with rapid recovery is different from weakening in HPT [17] where all hardness measurements after HPT processing are lower than in the original unprocessed material [36-39].

Numerous reports are now available showing conventional hardening without recovery in pure Cu [15,40-47] although there are two investigations showing the occurrence of softening when post-HPT annealing is conducted at elevated temperatures [35,48]. These results suggest, therefore, that the lower stacking fault energy of Cu prevents the occurrence of softening with rapid recovery as observed in high-purity Al. Nevertheless, a recent report described the use of oxygen free high conductivity (OFHC) Cu in experiments conducted at room temperature in repetitive upsetting-extrusion (RUE) where the material was subjected to repeated upsetting and extrusion [49]. In these experiments, the grain size of the Cu was refined from 150 μm to <2 μm and the microhardness was found to initially increase, reach a peak value and then decrease at low plastic strains to a saturation plateau. This behavior is similar to the softening with rapid recovery observed in the HPT processing of high purity Al and it suggests the same behavior may be observed in OFHC Cu if the HPT processing is conducted at low strains using fractional numbers of HPT turns.

Accordingly, the present investigation was initiated to examine the microstructural evolution in OFHC Cu processed by HPT using optical microscopy (OM), electron backscattered diffraction (EBSD) and the development of microhardness when processing by HPT at ambient temperature to different strain levels. The experiments used a very high purity Cu to facilitate the potential for dynamic recrystallization as reported in an earlier report on processing in the early stages of HPT straining [50]. Also, the use of a high purity material will provide information on the microstructures and microhardness that may be compared with other reports on Cu of lower purity.

2. Experimental material and procedures

The experiments were conducted with an OFHC copper of 99.99+ wt.% purity as used in an earlier study [50]: the chemical composition is given in Table 1. The material was received as a rod of 10 mm diameter and it was initially annealed for one hour at 673 K and then cut into disks with thicknesses of ~1.0 mm and polished on both sides using abrasive papers to final thicknesses of ~0.8 mm. The processing by HPT was conducted at ambient temperature under quasi-constrained conditions in which there is some limited outflow of material around the periphery of the disk between the two anvils [51]. All processing was conducted using an imposed pressure of 6.0 GPa and a rotation speed for the lower anvil of 1 rpm. The disks were processed through different numbers, N, of 1/4, 1/2, 1, 5 and 10 turns.

The HPT disks were prepared for microstructural examination with mirror-like surfaces using standard metallographic techniques. A Zeiss Axio-Imager optical microscope was used for the OM examinations and the samples were chemically etched at ambient temperature with a mixture of 50 ml of distilled water and 50 ml of nitric acid. Further microstructural evaluation was made using EBSD and this required electro-polishing in a solution of 25% phosphoric acid, 20% ethanol and 10% propanol in water. The grain boundary structures and microtextures were analyzed using an HKL Channel-5 EBSD

detector interfaced to a JOEL F7001 field-emission scanning electron microscope (SEM) operating at 20 kV. The EBSD data acquisition was made using Flamenco software. All EBSD measurements were performed on the disk plane at three different locations: the center, the mid-radius and a near-edge position. To incorporate microstructure evolution at different length scales, the EBSD maps were constructed using Tango software with step sizes in the range of 0.07–1.0 μm and subsequent microtexture analysis was performed using Mambo software. A minimum misorientation angle of 1° was used to quantify the grain size and grain boundary characteristics and all twins were included in the measurements. The misorientation angle distribution statistics were analyzed by employing a critical misorientation angle of 15° to differentiate between low-angle boundaries (LABs) and high-angle boundaries (HABs). The grain boundaries are presented in the EBSD maps with the LABs shown as thin grey lines, the HABs as solid black lines and the Σ3 twin boundaries as solid red lines. Detailed information on the average grain sizes and grain size distributions were also obtained using EBSD software.

All samples were mechanically ground and polished prior to measuring the Vickers microhardness, Hv. The indentations were made with a load of 200 gf and a dwell time of 15 s using a Buehler MicroMet Hardness Tester. As illustrated schematically in Figure 1, measurements were taken along four diameters arranged at 45° increments with the indentation points separated by 0.25 mm to a distance of 1.5 mm on eight sides of the center and separated by 0.5 mm thereafter. The microhardness was also measured at randomly selected positions for the annealed unprocessed condition. The results were plotted as the average microhardness values against the distances from the disk centers and the error bars were calculated at the 95% confidence limit.

3. Experimental results

3.1 Microstructural evolution

The microstructure of the Cu material in the annealed but unprocessed condition is shown by the OM micrograph and the EBSD map in Fig. 2. Due to the annealing treatment, the microstructure contains large grains with an average grain size of ~15.5 μm and with a high fraction of annealing twins with Σ3 boundaries.

Figure 3 presents a detailed montage of the microstructures from the EBSD mapping for samples processed from 1/4 to 10 turns in the vertical columns and at different radial positions corresponding to the center, mid-radius and near-edge in the top, middle and bottom rows, respectively. Higher magnification images are shown in Fig. 4 for the mid-radius and near-edge positions after 5 and 10 turns. In contrast to the relatively slow microstructural development at the centers of the disks, it is readily apparent that the degree of microstructural inhomogeneity at the mid-radius and near-edge positions decreases with increasing numbers of turns and this leads to ultrafine grains at high strains with an average grain size of ~0.3 μm in the near-edge position after 10 turns: a complete summary of the grain size measurements at all three positions is given in Table 2.

In the early stages of straining at N = 1/4 turn, the microstructure at the disk center in Fig. 3(a) contains a large fraction of LABs illustrating a typical strain hardening structure formed by cold working. However, there is evidence for dynamic recrystallization after 1/4 turn at the mid-radius and near-edge positions because of the presence of clusters of ultra-fine grains in Fig. 3(b) and (c). This recrystallization gives average grain sizes of ~1.16 and ~0.75 μm at these two positions, respectively. At N = 1/2 and 1 turn, there is an increase in the density of these clusters of ultrafine grains as shown in Fig. 3(e,f,h,i) while the microstructures at the centers of both disks remain essentially unchanged in Fig. 3(d,g). Full refinement of the microstructure is evident in Fig. 3(k,l,n,o) and Fig. 4 for the mid-radius and near-edge positions after processing through 5 and 10 turns whereas the microstructures at the disk centers contain a mixture of recrystallized grains and clusters of ultrafine grains after

5 and 10 turns in Fig. 3(j, m). These results are consistent with data recorded earlier for OFHC Cu [50].

Inspection of the average grain sizes in Table 2 shows that the smallest sizes occur consistently in the near-edge positions with the largest grain sizes in the centers. Even after 10 turns, the average grain size at the center of the disk is close to ~1 μm so that the material fails to attain a true homogeneous steady-state condition when processing through 10 turns. Although most materials appear to reach a saturation in microhardness after reasonably large numbers of turns, there are direct reports of a lack of microhardness saturation after 40 turns in a NiTi alloy [52] and 50 turns in a β-titanium alloy [53].

Table 3 shows the measured length fractions of HABs and Σ3 twin boundaries for each of the conditions shown in Fig. 3. There is a high fraction of Σ3 boundaries of ~49% and ~59% at N = 1/4 turn for the mid-radius and near-edge positions, respectively, and there are also very high fractions of ~76% and ~89% of HABs in these two positions after 1/4 turn. These results are consistent with the advent of dynamic recrystallization in the very earliest stages of HPT processing. After 1/2 turn, the fraction of Σ3 boundaries further increases to ~55% at the mid-radius position but decreases to ~14% at the near-edge position due to the increasing numbers of ultrafine grain clusters. At the same time the fraction of HABs in the near-edge position is reduced to ~69%. Finally, further straining to 10 turns leads to a slight reduction in the fraction of HAB to ~57% but with a very significant reduction in the fraction of Σ3 boundaries to ~5% at both the mid-radius and near-edge positions, respectively. By contrast, the center of the disk contains low fractions of ~15% and ~3 %, respectively, of HAB and Σ3 boundaries after 1/4 to 1 turn which confirms the dominance of the LABs associated with the initial subgrain structure. There is no evidence for ultrafine grain refinement at the centers of the disks until 5 turns where the fractions of HABs and Σ3 boundaries increases to ~50% and

~14%, respectively. These results suggest that the formation of Σ3 boundaries moves from the periphery towards the center of the disk with increasing numbers of HPT turns.

3.2 Microhardness measurements

The average values of Hv obtained from linear traverses along disk diameters are plotted against the positions on the disks as shown in Fig. 5 for (a) 1/4, (b) 1/2, (c) 1, (d) 5 and (e) 10 turns: in all plots the average hardness for the annealed unprocessed sample is given by the lower line at Hv ≈ 48.

Inspection shows these hardness measurements are different by comparison with all values of Hv reported in earlier investigations of the microhardness values after processing by HPT as summarized in a recent review [17]. First, at N = 1/4 turn in Fig. 5(a) the microhardness value is ~90 Hv in the center of the disk, increases to a peak value of ~150 Hv at displacements of ~1.5 mm from the center and then drops to ~80 Hv at larger distances. This variation in hardness with distance has similarities to earlier reports of hardness versus distance for high purity Al [18,21]. After 1/2 turn in Fig. 5(b), the maximum peaks at ~150 Hv are displaced to positions at ~1 mm on either side of the center and the hardness at the edge also increases to a maximum value of ~110 Hv. Straining by HPT to 1 turn in Fig. 5(c) displaces the peaks in the central area to ~0.5 mm on either side of the center and the hardness at the edge increases to ~145 Hv. At 5 turns in Fig. 5(d), the variation looks similar to most f.c.c. metals with the hardness values attaining a reasonable steady-state value of ~150 Hv at points at and beyond ~0.5 mm from the disk center with a lower hardness of ~120 Hv in the center. Finally, at 10 turns in Fig. 5(e), there is a reasonable level of homogeneity across most of the disk with a hardness of ~150 Hv but in the center there is a lower hardness at ~135 Hv.

4. Discussion

4.1 Microstructural evolution in OFHC Cu processed by HPT

The results show the microstructures in OFHC Cu evolve rapidly in the early stages of straining as demonstrated by observations taken along radial positions within the disks. In the initial stages of straining, the microstructure undergoes typical strain hardening associated with the formation of LABs and subgrains. This is followed by dynamic recrystallization and the formation of Σ3 twin boundaries, leading ultimately to an array of ultra-fine grains at even higher strains.

The limited microstructural evolution occurring near the centers of the disks in the early stages of straining, as shown in Fig. 3(a,d,g), is typical of many metals processed by HPT and the effect is generally attributed primarily to the compressive strain rather than the torsional strain [54]. However, at 5 and 10 turns the torsional strain dominates resulting in significant microstructural and hardness changes as shown by the development of recrystallized grains and ultra-fine grains at distances of ~50 to 100 μm from the disk center in Fig. 3(j,m). The formation of recrystallized grains near the centers of the disks, together with the presence of unsheared regions, supports the lower values of microhardness (~120-135 Hv) by comparison with the steady-state hardness of ~150 Hv. This is also supported by the results in Table 2 which show the average grain size in the central region decreases to ~0.97 μm after 10 turns but remains larger than the steady-state grain size of ~0.3 μm.

4.2 Characteristics of hardening in OFHC Cu processed by HPT

When hardness measurements are taken after different numbers of turns in HPT processing, the average values increase with increasing strain but there is generally an apparent scatter in the individual datum points. It was shown in an early investigation of HPT processing of an austenitic steel that all of the hardness values may be conveniently correlated onto a single curve by plotting the individual values against the equivalent strain calculated using eq. (1) [16]. An example of this type of plot is shown in Fig. 6 where all of

the individual points are taken directly from Fig. 5. This plot shows that the hardness initially increases, then decreases to a lower level and finally increases again and ultimately reaches a reasonable saturation condition at equivalent strains of ~20 and higher.

In order to more fully display the variation of microhardness with equivalent strain in the very early stages of HPT processing, the same datum points are replotted in Fig. 7 where the equivalent strain is now on a logarithmic scale from 0.1 to 1000. Thus, the microhardness increases to a maximum value of ~150 Hv at an equivalent strain of ~2, decreases in the range of $\varepsilon_{eq} \approx$ 3-8 and thereafter increases to a steady-state level at ~150 Hv at equivalent strains above ~22.

Figure 7 is unusual because there is a drop in hardness and the hardness values remain constant at ~80 Hv over equivalent strains from ~3 to ~8. This drop is related to the onset of dynamic recrystallization which is first apparent near the edge at small strains and then moves inwards towards the center of the disk with further straining. The shift in recrystallization from the periphery towards the center is consistent with earlier observations on OFHC Cu processed by HPT [50]. Using eq. (1), the equivalent strain for N = 1/4 turn is ~2.8 at the mid-radius position and ~5.7 at the near-edge. This leads to softening to the minimum value as shown in Fig. 5(b) with the softening starting at about 2.5 mm from the center of the disk and extending to the periphery. At N = 1/2 turn, the equivalent strain is ~5.7 at the mid-radius and ~11.3 at the near-edge. This is shown in Fig. 5(c) where the hardness remains at a minimum of ~80 Hv at 2.5 mm but increases to ~110 Hv at the edge and it is consistent with the microstructural evolution in Fig. 3(e,f) where recrystallized grains prevail at the mid-radius position while several clusters of ultra-fine grains develop in the recrystallized microstructure at the near-edge position. In the case of N = 1 turn, the equivalent strain is ~11.3 at the mid-radius and ~22.7 at the near-edge. This increase in strain affects the microhardness evolution presented in Fig. 5(d) where it increases to about 95 Hv

at the mid-radius at 2.5 mm and becomes ~145 Hv at the periphery. As shown in Fig. 6, the microhardness gradually reaches the steady-state level of ~150 Hv at ε_{eq} >22 and this is also supported by the EBSD map for the near-edge position at N = 1 turn in Fig. 3(i) where almost complete grain refinement is achieved. Nevertheless, the microstructure at mid-radius shown in Fig. 3(h) continues to evolve as shown by the formation of ultra-fine grain clusters within the recrystallized structure. Further straining to N = 5 and 10 turns produces an ultra-fine grain structure almost everywhere except at the center of the disk.

The recent study on OFHC Cu using the RUE process at ambient temperature showed that the numbers of clusters of fine recrystallized grains increased with increasing numbers of RUE cycles [49]. This was accompanied by a drop in the microhardness to ~67 Hv over equivalent strains between 3 and 10 and thereafter there was an increase to a maximum hardness of ~130 Hv. The drop in microhardness was attributed to a rapid reduction in the dislocation density due to a decrease in the output of Frank-Read sources within the grains with decreasing grain size [55] and a similar explanation may be invoked in the present experiments as an explanation for the behavior shown in Fig. 7.

4.3 Comparisons with Cu of lower purity processed by HPT

A comparison with earlier studies on HPT of pure Cu of 99.99% purity or lower [46,56-58] reveals three important differences in the current study using very high purity OFHC Cu: (1) the present results show a local maximum microhardness at a very low equivalent strain of ~2, (2) thereafter the microhardness decreases to a new local minimum at equivalent strains between ~3 and ~8 and (3) the steady-state microhardness begins at equivalent strain above ~22 whereas it occurred at equivalent strains above ~15 in the earlier studies on lower purity material [56,57].

These differences are due to dynamic recrystallization which occurs in the present investigation at $\varepsilon_{eq} \approx 3$ to 8. In some studies of the HPT of pure Cu it was assumed that

recrystallization occurred during straining due to the occurrence of adiabatic heating during the shearing process [59,60] since it is now well established that there may be significant heating during HPT processing [61]. Nevertheless, the present results suggest another important factor because of the enhancement of dislocation mobility which follows from the reduction in the impurity concentration in the very pure Cu. In HPT of high purity Al (99.99%) [18], both the SFE and the homologous testing temperature were high and this eases the dislocation movement and leads to a faster accumulation of dislocations during the early stages of straining and an enhanced formation of subgrain boundaries. Similarly, the presence of very few impurities in the OFHC Cu of 99.99%+ purity facilitates dislocation mobility and promotes the rapid formation of subgrain boundaries in the early stages of straining with the occurrence of dynamic recovery and recrystallization at $\varepsilon_{eq} \approx 3$. This also produces a large increase in the length fraction of Σ3 boundaries during the early stages of HPT straining as shown by the fractions of ~50% recorded in Table 3 after N = 1/4 turn.

The present results are consistent with other studies evaluating the effects of impurities. For example, an EBSD study on the effect of purity on the hot working behavior of different austenitic stainless steels showed that dynamic recrystallization started earlier and at lower testing temperatures in the high purity steel by comparison with other steels having higher carbon contents [62]. This was attributed to the easier dislocation movement in the high purity steel leading to greater grain boundary mobility and a higher probability of twin boundary generation. Similarly, an investigation of the role of orientation pinning by neighboring grains on migrating boundaries in a statically recrystallized OFHC copper showed that some recrystallized grains with Σ3 boundaries exerted the greatest pinning effect on the growing grains [63]. Adopting a similar analogy in the present experiments, it is proposed that the low mobility of the Σ3 boundaries, which are formed by dynamic recrystallization in the early stage of HPT straining, produces a resistance to excessive grain

growth of the recrystallized grains and therefore the material becomes susceptible to dislocation accumulation followed by subgrain formation with additional shearing. This leads to clusters of ultra-fine grains at the expense of the recrystallized grain as shown in Fig. 3. At higher HPT strains, as after 5 and 10 turns, full grain refinement occurs at the mid-radius and near-edge positions and the material behaves as in conventional HPT processing. In addition, it should be noted that some grains at high strains are relatively coarse and contain Σ3 boundaries, thereby demonstrating that dynamic recrystallization and grain growth occur but to a lesser extent than in the early stages of straining.

5. Summary and conclusions

1. Experiments were conducted to evaluate the microstructure and microhardness evolution during the HPT processing of OFHC copper of 99.99wt.%+ purity.

2. In the early stages of straining, after 1/4 to 1 turn, dynamic recrystallization occurs at the mid-radius and near-edge positions producing a large fraction of Σ3 twin boundaries. Ultrafine grains are produced in the recrystallized microstructure with increasing amounts of strain.

3. Hardness measurements show that the occurrence of dynamic recrystallization, followed by ultrafine-grain refinement, shifts from the periphery towards the center of the disk with further straining. The microhardness reaches a maximum of ~150 Hv at an equivalent strain of ~2, then decreases to a minimum of ~80 Hv up to an equivalent strain of ~8 and thereafter it increases to a steady-state level of ~150 Hv for equivalent strains >22.

4. The high purity of the Cu promotes dislocation mobility and this enhances the occurrence of dynamic recrystallization and dynamic softening at low strains. This leads to the present results which are consistent with earlier experiments conducted using repetitive upsetting-extrusion.

Acknowledgements

The authors acknowledge the support provided by the Public Authority of Applied Education and Training (Grant No. TS-12-03) and Kuwait University General Facility (Grant No. GE 01/07) for sample preparation, OM and EBSD measurements. This work was supported in part by the European Research Council under ERC Grant Agreement No. 267464-SPDMETALS.

References

[1] R.Z. Valiev, R.K. Islamgaliev, I.V. Alexandrov, Prog. Mater. Sci. 45 (2000) 103.

[2] R.Z. Valiev, I. Sabirov, A.P. Zhilyaev, T.G. Langdon, JOM 64 (2012) 1134.

[3] Y. Estrin, A. Vinogradov, Acta Mater. 61 (2013) 782.

[4] R.Z. Valiev, Y. Estrin, Z. Horita, T.G. Langdon, M.J. Zehetbauer, Y.T. Zhu, JOM 58(4) (2006) 33.

[5] Y. Zhu, R.Z. Valiev, T.G. Langdon, N. Tsuji, K. Lu, MRS Bull. 35 (2010) 977.

[6] T.G. Langdon, Acta Mater. 61 (2013) 7035.

[7] R.Z. Valiev, T.G. Langdon, Prog. Mater. Sci. 51 (2006) 881.

[8] A.P. Zhilyaev, T.G. Langdon, Prog. Mater. Sci. 53 (2008) 893.

[9] A.P. Zhilyaev, S. Lee, G.V. Nurislamova, R.Z. Valiev, T.G. Langdon, Scripta Mater. 44 (2001) 2753.

[10] A.P. Zhilyaev, B.K. Kim, G.V. Nurislamova, M.D. Baró, J.A. Szpunar, T.G. Langdon, Scripta Mater. 46 (2002) 575.

[11] J. Wongsa-Ngam, M. Kawasaki, T.G. Langdon, J. Mater. Sci. 48 (2013) 4653.

[12] R.Z. Valiev, Yu.V. Ivanisenko, E.F. Rauch, B. Baudelet, Acta Mater. 44 (1996) 4705.

[13] A.P. Zhilyaev, G.V. Nurislamova, B.K. Kim, M.D. Baró, J.A. Szpunar, T.G. Langdon, Acta Mater. 51 (2003) 753.

[14] Y. Estrin, A. Molotnikov, C.H.J. Davies, R. Lapovok, J. Mech. Phys. Solids 56 (2008) 1186.

[15] H. Jiang, Y.T. Zhu, D.P. Butt, I.V. Alexandrov, T.C. Lowe, Mater. Sci. Eng. A290 (2000) 128.

[16] A. Vorhauer, R. Pippan, Scripta Mater. 51 (2004) 921.

[17] M. Kawasaki, J. Mater. Sci. 49 (2014) 18.

[18] C. Xu, Z. Horita, T.G. Langdon, Acta Mater. 55 (2007) 203.

[19] Y. Ito, Z. Horita, Mater. Sci. Eng. A503 (2009) 32.

[20] C. Xu, Z. Horita, T.G. Langdon, Mater. Trans. 51 (2010) 2.

[21] M. Kawasaki, R.B. Figueiredo, T.G. Langdon, Acta Mater. 59 (2011) 308.

[22] A.P. Zhilyaev, K. Oh-ishi, T.G. Langdon, T.R. McNelley, Mater. Sci. Eng. A410-411 (2005) 277.

[23] C. Xu, Z. Horita, T.G. Langdon, Acta Mater. 56 (2008) 5168.

[24] Y. Harai, K. Edalati, Z. Horita, T.G. Langdon, Acta Mater. 57 (2009) 1147.

[25] Z.C. Duan, X.Z. Liao, M. Kawasaki, R.B. Figueiredo, T.G. Langdon, J. Mater. Sci. 45 (2010) 4621.

[26] A. Loucif, R.B. Figueiredo, T. Baudin, F. Brisset, T.G. Langdon, Mater. Sci. Eng. A527 (2010) 4864.

[27] V. Rajinikanth, K. Venkateswarlu, M.K. Sen, M. Das, S.N. Alhajeri, T.G. Langdon, Mater. Sci. Eng. A528 (2011) 1702.

[28] S. Sabbaghianrad, M. Kawasaki, T.G. Langdon, J. Mater. Sci. 47 (2012) 7789.

[29] A. Loucif, R.B. Figueiredo, T. Baudin, F. Brisset, R. Chemam, T.G. Langdon, Mater.

Sci. Eng. A532 (2012) 139.

[30] T. Mungole, N. Nadammal, K. Dawra, P. Kumar, M. Kawasaki, T.G. Langdon, J. Mater. Sci. 48 (2013) 4671.

[31] X. Xu, Q. Zhang, N. Hu, Y. Huang, T.G. Langdon, Mater. Sci. Eng. A588 (2013) 280.

[32] S. Sabbaghianrad, T.G. Langdon, Mater. Sci. Eng. A596 (2014) 52.

[33] P. Bazarnik, Y. Huang, M. Lewandowska, T.G. Langdon, Mater. Sci. Eng. A626 (2015) 9.

[34] K. Edalati, A. Yamamoto, Z. Horita, T. Ishihara, Scripta Mater. 64 (2011) 880.

[35] K. Edalati, Z. Horita, Mater. Sci. Eng. A528 (2011) 7514.

[36] M. Kawasaki, B. Ahn, T.G. Langdon, Acta Mater. 58 (2010) 919.

[37] M. Kawasaki, B. Ahn, T.G. Langdon, Mater. Sci. Eng. A527 (2010) 7008.

[38] N.X. Zhang, M. Kawasaki, Y. Huang, T.G. Langdon, J. Mater. Sci. 48 (2013) 4582.

[39] T.S. Cho, H.J. Lee, B. Ahn, M. Kawasaki, T.G. Langdon, Acta Mater. 72 (2014) 67.

[40] A. Dubravina, M.J. Zehetbauer, E. Schafler, I.V. Alexandrov, Mater. Sci. Eng. A387-389 (2004) 817.

[41] Z. Horita, T.G. Langdon, Mater. Sci. Eng. A410-411 (2005) 422.

[42] X.H. An, S.D. Wu, Z.F. Zhang, R.B. Figueiredo, N. Gao, T.G. Langdon, Scripta Mater. 63 (2010) 560.

[43] J. Čížek, M. Janeček, O. Srba, R. Kužel, Z. Barnovská, I. Procházka, S. Dobatkin, Acta Mater. 59 (2011) 2322.

[44] J. Čížek, O, Melikhova, M. Janeček, O. Srba, Z. Barnovská, I. Procházka, S. Dobatkin, Scripta Mater. 65 (2011) 171.

[45] K. Edalati, K. Imamura, T. Kiss, Z. Horita, Mater. Trans. 53 (2012) 123.

[46] K. Edalati, Z. Horita, T. Furuta, S. Kuramoto, Mater. Sci. Eng. A559 (2013) 506.

[47] A.P. Zhilyaev, A.A. Gimazov, T.G. Langdon, J. Mater. Sci. 48 (2013) 4461.

[48] K. Edalati, Y. Ito, K. Suehiro, Z. Horita, Int. J. Mater. Res. 100 (2009) 1668.

[49] I. Balasundar, K.R. Ravi, T. Raghu, Mater. Sci. Eng. A583 (2013) 114.

[50] K.J. Al-Fadhalah, S.N. Alhajeri, A.I. Almazrouee, T.G. Langdon, J. Mater. Sci. 48 (2013) 4563.

[51] R.B. Figueiredo, P.H.R. Pereira, M.T.P. Aguilar, P.R. Cetlin, T.G. Langdon, Acta Mater. 60 (2012) 3190-3198.

[52] H. Shahmir, M. Nili-Ahmadabadi, Y. Huang, T.G. Langdon, J. Mater. Sci. 49 (2014) 2998.

[53] K. Sharman, P. Bazarnik, T. Brynk, A.G. Bulutsuz, M. Lewandowska, Y. Huang, T.G. Langdon, J. Mater. Res. Tech. 4 (2015) 79-83.

[54] Y. Song, E.Y. Yoon, D.J. Lee, J.H. Lee, H.S. Kim, Mater. Sci. Eng. A528 (2011) 4840.

[55] N.A. Enikeev, H.S. Kim, I.V. Alexandrov, Mater. Sci. Eng. A460–461 (2007) 619.

[56] K. Edalati, T. Fujioka, Z. Horita, Mater. Sci. Eng. A497 (2008) 168.

[57] X.H. An, S.D. Wu, Z.F. Zhang, R.B. Figueiredo, N. Gao, T.G. Langdon, Scripta Mater. 63 (2010) 560.

[58] K. Edalati, Z. Horita, Mater. Trans. 51 (2010) 1051.

[59] A.P. Zhilyaev, T.R. McNelley, T.G. Langdon, J. Mater. Sci. 42 (2007) 1517.

[60] A.P. Zhilyaev, S. Swaminathan, A.A. Gimazov, T.R. McNelley, T.G. Langdon, J. Mater. Sci. 43 (2008) 7451.

[61] P.H.R. Pereira, R.B. Figueiredo, Y. Huang, P.R. Cetlin, T.G. Langdon, Mater. Sci. Eng. A593 (2014) 185.

[62] M. El Wahabi, L. Gavard, J.M. Cabrera, J.M. Prado, F. Montheillet, Mater. Sci. Eng. A393 (2005) 83.

[63] D.R. Waryoba, P.N. Kalu, A.D. Rollett, Metall. Mater. Trans. A 36A (2005) 205.

Table.1 Chemical composition of OFHC copper (wt.%)

Sample/El	Ag	As	Bi	Cd	Fe	Mn	I	O	P	Pb	S	Sb	Se	Sn	Te	Zn	Cu
OFHC Cu	0.00	0.00	0.00	0.00	0.0	0.000	0.0	0.00	0.00	0.00	0.00	0.00	0.00	0.00	0.00	0.00	99.9*

* Minimum guaranteed percentage of Cu

Table 2 EBSD grain size measurements of HPT Cu samples

Sample	Average grain size (μm)		
	Center	Mid-radius	Near-edge
N = 1/4	6.85	1.16	0.75
N = 1/2	5.38	0.55	0.34
N = 1	4.71	0.44	0.32
N = 5	1.52	0.38	0.37
N =10	0.97	0.34	0.28

Table 3 Length fractions of HABs and Σ3 twin boundaries

Sample	Length fraction of grain boundaries (%)					
	Center		Mid-radius		Near-edge	
	HABs	Σ 3	HABs	Σ 3	HABs	Σ 3
N = 1/4	15.5	3.0	76.0	49	89.2	59
N = 1/2	13.9	3.3	82.6	55.1	69.5	13.7
N = 1	15.2	2.12	80.6	38.2	63.0	7.0
N = 5	50.2	13.9	62.0	4.42	64.1	4.3
N =10	33.8	5.5	56.3	4.5	56.6	4.8

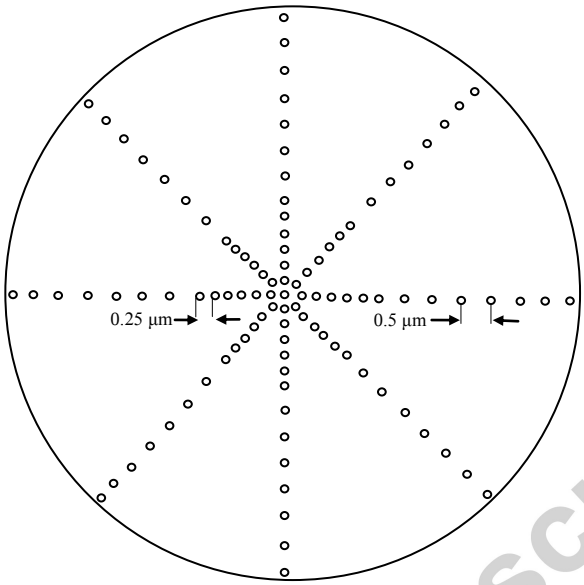

Figure 1. Schematic illustration of the microhardness measurement positions across the diameters of disks after HPT

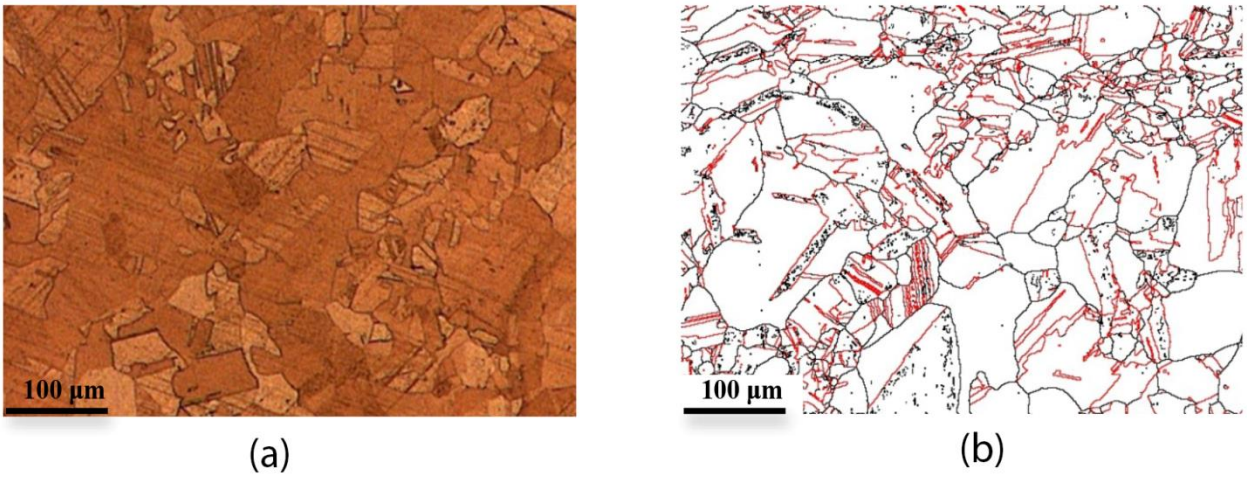

Figure 2. Microstructure of unprocessed annealed pure Cu (**a)** optical micrograph, (**b)** grain boundary reconstruction from EBSD mapping: black lines denote random HABs and red lines represent Σ3 boundaries.

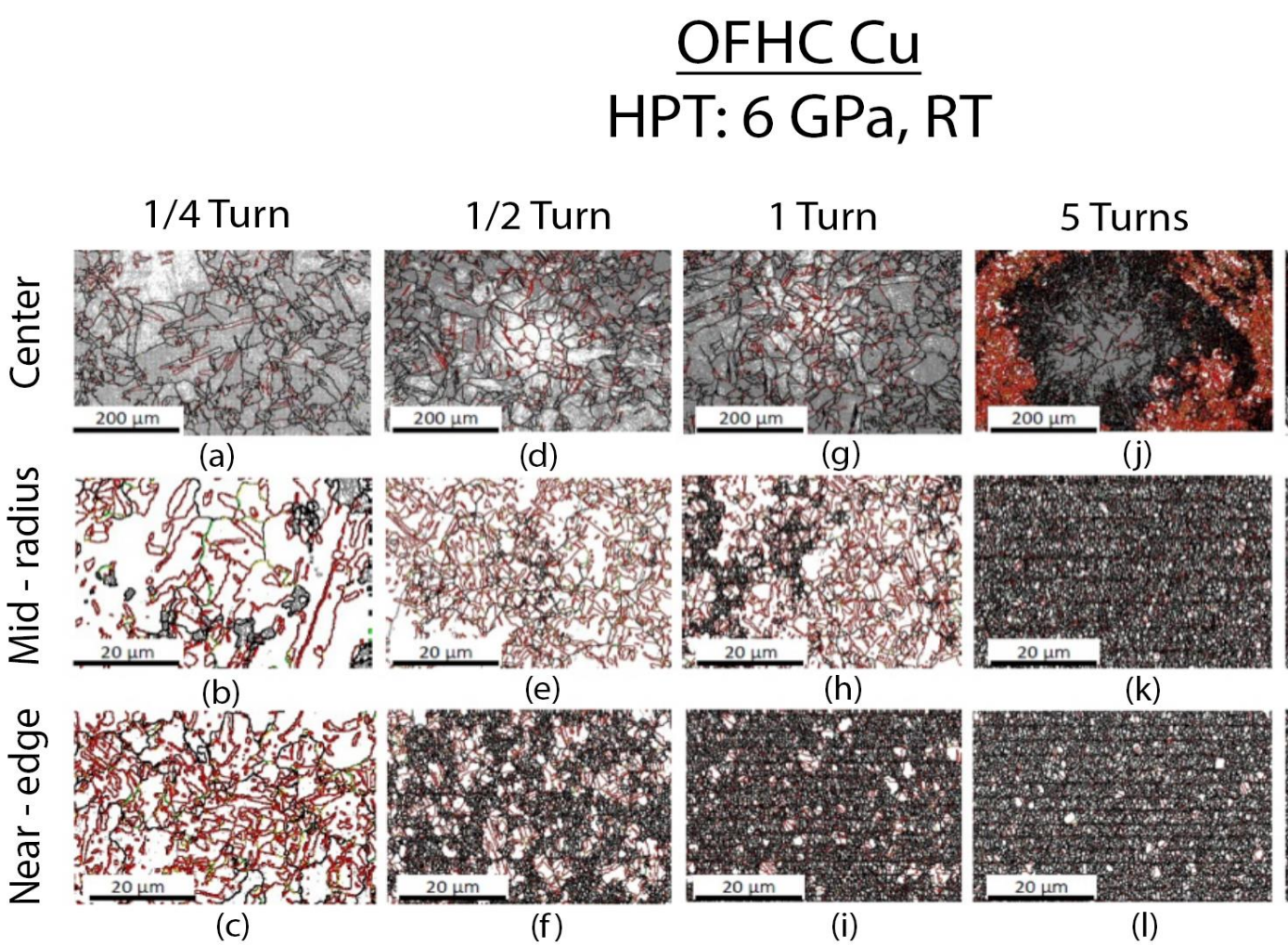

Figure 3. Grain boundary reconstruction from EBSD mapping for samples processed at (a–c) 1/4, (d–f) 1/2, (g–i) 1, (j–l) 5 and (m
LABs, black lines denote random HABs and red lines represent Σ3 boundaries

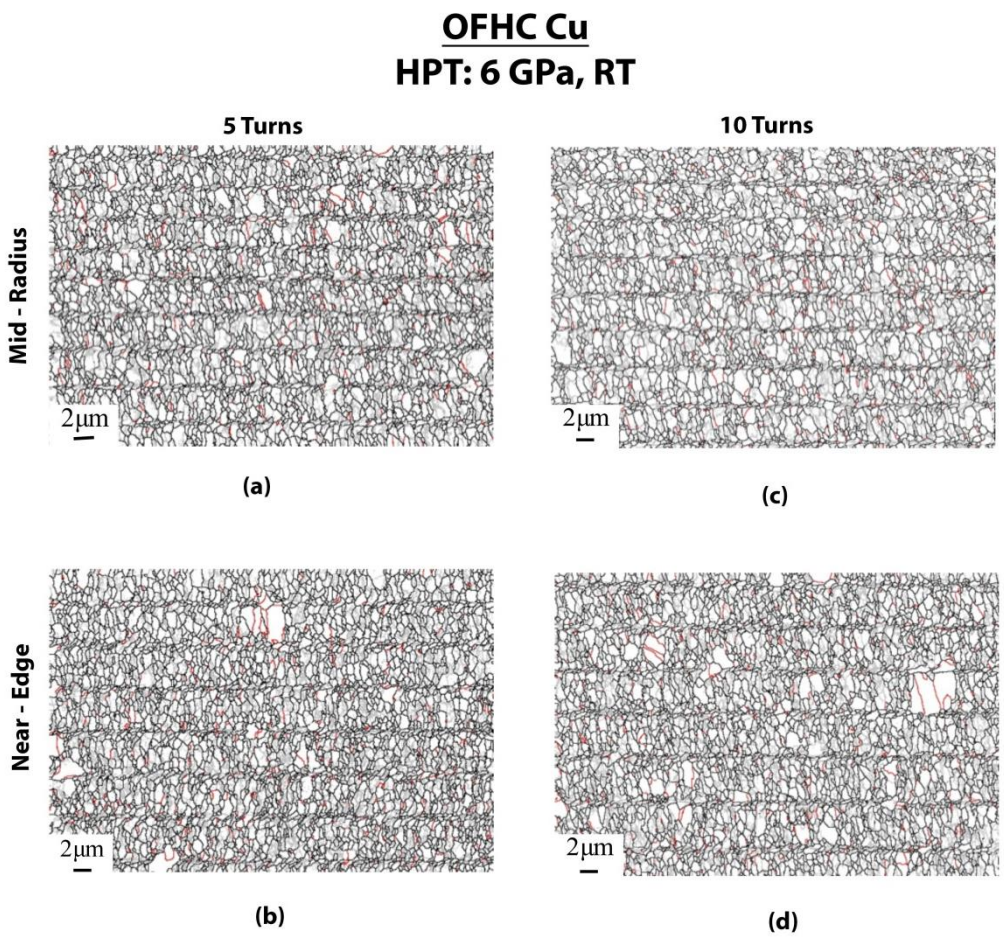

Figure 4 Higher magnification images illustrating grain refinement for the samples processed by (a-b) 5 and (c-d) 10 turns: grey lines denote LABs, black lines denote random HABs and red lines represent Σ3 boundaries.

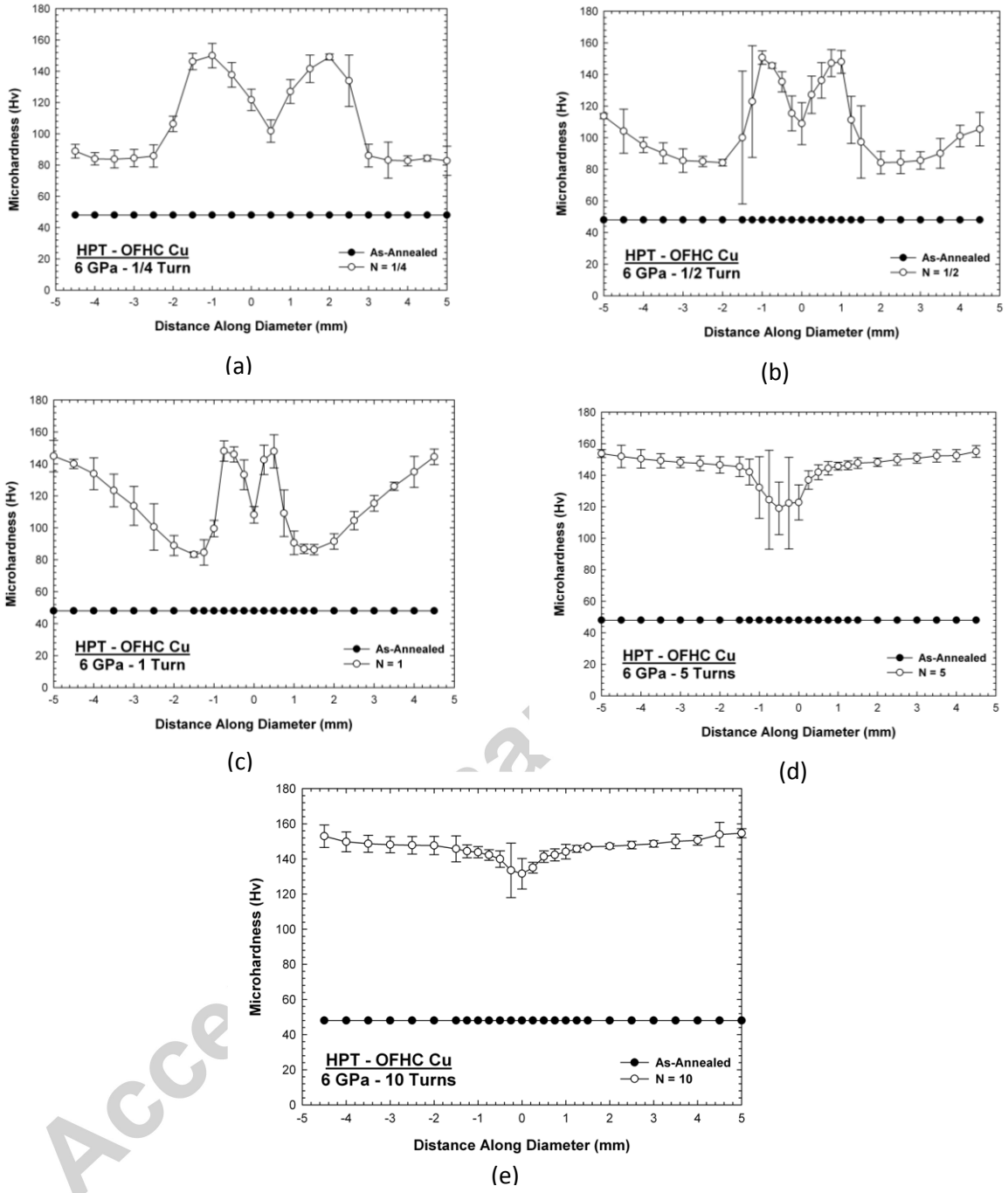

Figure 5. The average microhardness compared with the annealed condition, Hv, versus distance along diameter at (a) 1/4 turn, (b) 1/2 turn, (c) 1 turn, (d) 5 turns and (e) 10 turns.

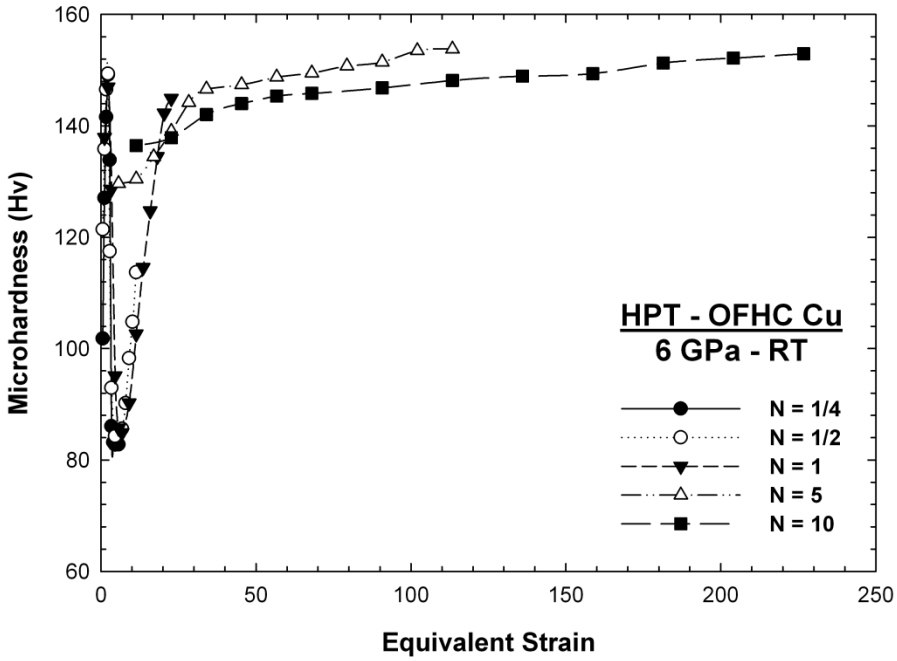

Figure 6. Average Vickers microhardness of OFHC Cu after HPT plotted against the equivalent strain.

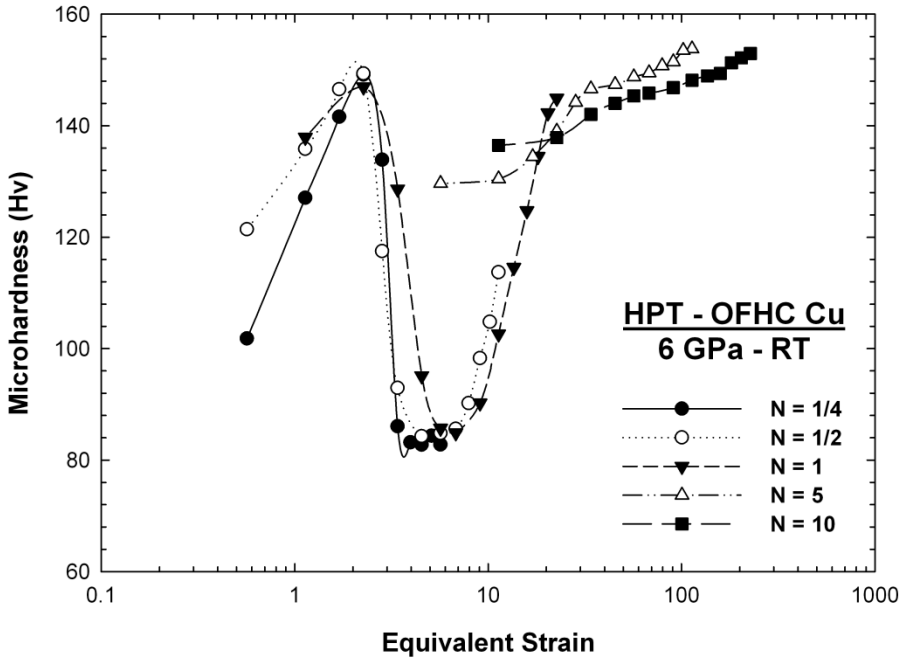

Figure 7. Average Vickers microhardness of OFHC Cu after HPT plotted against the equivalent strain on a logarithmic scale.